Electronic structure of Ni_3Al and $NiAl_3$ alloys: X-ray-absorption fine-structure analysis

A. N. Mansour*
Naval Surface Warfare Center, Carderock Division, Code 684, 9500 MacArthur Boulevard, West Bethesda, Maryland 20817-5700

A. Dmitrienko and A. V. Soldatov†
Department of Solid State Physics, Rostov University, Sorge Street 5, Rostov-Don, 344090, Russia
(Received 21 February 1997)

X-ray-absorption fine structure (XAFS) above the Ni K edge in Ni_3Al and $NiAl_3$ alloys has been measured and theoretical full multiple-scattering analysis of these data have been done. The theoretical XAFS are found to be in agreement with experimental data. The XAFS of Ni_3Al and $NiAl_3$ alloys are rather different. Since the dipole transition matrix element is not a very sharp function of the energy the experimental XAFS reflects the averaged in space partial Ni p unoccupied states in the conduction bands of the Ni_3Al and $NiAl_3$ alloys, showing changes in the electronic structure going from Ni_3Al to $NiAl_3$ alloy. Theoretical partial density of states curves calculated along the axis parallel to the c vector differ from the partial density of states curves calculated in the ***ab*** plane for both alloys. [S0163-1829(97)01724-4]

INTRODUCTION

The Ni_3Al and $NiAl_3$ compounds and in general nickel-based superalloys, due to their unique high-temperature physical and mechanical properties, have been of much interest in recent years because of their potential applications in advanced material technology.[1] Currently, this class of intermetallic alloys is being examined for use in diesel engine turbocharger rotors, high-temperature die and molds, hydroturbines, and cutting tools. The unique properties of Ni_3Al and $NiAl_3$ compounds are due, in part, to the nature of their atomic/crystal and electronic structures. While crystal structure of these compounds is well understood, the electronic structure of Ni_3Al and $NiAl_3$ has been studied both experimentally and theoretically, but mostly in the occupied part of the electronic states. Electronic heat capacity of NiAl alloys analysis has been used for the study of the density of states at the Fermi level.[2] On the basis of the ''compressed atoms'' approach partial occupation numbers of electronic states have been calculated for NiAl, Ni_3Al, and $NiAl_3$.[3] The electronic structure of NiAl alloys has been investigated by using x-ray photoelectron spectroscopy (XPS) spectra of valence bands,[4] XPS of core (Ni $2p$) levels[5] and Ni L_3VV Auger spectra.[6] Al $L_{2,3}$ x-ray emission bands have been measured in a series of NiAl alloys.[7] A band-structure calculation allowed determination of the density of states as a function of energy[8] and multielectron approximation has been used for the study of hybridization of Al p and Ni d bands.[9] Recently, occupied states in Ni_3Al and $NiAl_3$ alloys have been studied using Al $KL_{2,3}V$ and Ni LMM Auger lines, high-resolution XPS valence-band spectra, and theoretical discrete variation $X\alpha$ cluster calculation.[10] But the lack of information on the unoccupied Ni p states in Ni_3Al and $NiAl_3$ is a severe limitation due to the importance of the unoccupied states at the bottom of the conduction band in order to account for the physical properties of these alloys.

In this paper, we have measured the Ni K-edge x-ray-absorption fine structure (XAFS) of Ni_3Al and $NiAl_3$ and applied the multiple-scattering approach analysis in real space in order to study the fine structure of unoccupied electronic Ni p states in the conduction band of these alloys. Our task is to study the difference between the electronic structures of Ni_3Al and $NiAl_3$ using full multiple-scattering analysis of XAFS. The full multiple-scattering analysis has been applied to interpret a large number of XAFS in various materials (see for a review Refs. 11 and 12) but no multiple-scattering calculations in real space have been applied to the study of unoccupied states in Ni_3Al and $NiAl_3$.

EXPERIMENT AND METHOD OF CALCULATION

The x-ray-absorption experiments were performed on beamline X-11A of the National Synchrotron Light Source at Brookhaven National Laboratory with the electron storage ring operating at an electron energy of 2.528 GeV and a stored current in the range of 110–300 mA.[13] Data were collected with a variable exit double-crystal monochromator using two flat Si(111) crystals. Harmonics were rejected by detuning the parallelism of the crystals. The x-ray intensities were monitored using ionization chambers filled with nitrogen gas for the incident beam and a mixture of argon (15%) and nitrogen (85%) gases for the transmitted beam.

To minimize the effect of particle size on XAFS amplitudes,[14] powdered samples were prepared by grinding and sieving through a 20-μm-size nylon screen. The fine powder was then deposited on Kapton tape and few layers were stacked to give a relatively uniform thickness with an x-ray-absorption edge jump, $\Delta\mu x$, of 1.44 for Ni_3Al and 0.90 for $NiAl_3$. The room-temperature XAFS spectra were measured in the transmission mode. A 4-μm-thick Ni Foil (99.95% purity) purchased from Goodfellow (Cambridge Science Park, UK) with a $\Delta\mu x$ of 1.07 was used as a reference for energy calibration. The x-ray-absorption edge jump for each sample was kept below 1.5 in order to minimize the thickness effect.[15] The pre-edge background absorption was determined from a quadratic fit to the data from about 300 to

TABLE I. Structure of the four-shell cluster around the central atom of Ni for Ni_3Al (total number of atoms is 55).

Shell number	Atom type	Coordination number	Radius (Å)
1	Al	4	2.5212
1	Ni	8	2.5212
2	Ni	6	3.5655
3	Ni	16	4.3668
3	Al	8	4.3668
4	Ni	12	5.0424

30 eV below the edge energy and then extrapolating over the entire energy range of the spectrum. An energy-independent step normalization was applied by dividing by the value of the post-edge atomic absorption at 100 eV above the edge energy. The energy resolution in the measured interval is about 1.0 eV.

The algorithm of the full multiple-scattering method we used in this study has been described earlier.[16] We treated the Ni_3Al alloy as having ordered Cu_3Au crystal structure with a lattice constant equal to 3.5655 Å.[17] The $NiAl_3$ alloy has a lower symmetry structure.[17] The clusters of neighbor atoms around the central Ni atom were divided into shells as reported in Table I for the Ni_3Al alloy and in Table II for the $NiAl_3$ alloy. Phase shifts were calculated in the crystal muffin-tin (MT) potential with touching MT spheres. The muffin-tin radii and the muffin-tin constants that we have obtained according to our procedure of the muffin-tin potential construction[16] are reported in Table III. We have used

TABLE II. Structure of the four-shell cluster around the central atom of Ni for $NiAl_3$ (total number of atoms is 42).

Shell number	Atom type	Coordination number	Radius (Å)
1	Al	2	2.4218
1	Al	2	2.4452
1	Al	1	2.4484
1	Al	1	2.4609
1	Al	2	2.5210
1	Al	1	2.7173
2	Ni	2	3.8011
2	Al	2	3.8830
2	Ni	2	4.1044
2	Al	2	4.1466
3	Al	2	4.2451
3	Al	1	4.2976
3	Ni	2	4.4205
3	Al	2	4.4607
3	Al	2	4.4625
4	Al	2	4.6669
4	Ni	4	4.6721
4	Al	2	4.7054
4	Al	1	4.7668
4	Ni	2	4.8112
4	Al	2	4.8376
4	Al	2	4.8658

TABLE III. The muffin-tin radii R_{MT} of the atoms included and the muffin-tin constants V_0 of the potential used in the calculation.

	Ni_3Al		$NiAl_3$	
Atom	R_{MT} (Å)	V_0 (eV)	R_{MT} (Å)	V_0 (eV)
Ni	1.2478	−20.75	1.2291	−19.33
Al	1.0987	−20.70	1.1876	−19.26

the muffin-tin approximation according to the Mattheiss prescription with exchange parameter equal to 1.0 while constructing the crystal potential. Atomic-charge densities were obtained with the help of the self-consistent Dirac-Slater method.

It is well known now that XAFS above the K edge of solid matter is generated by multiple scattering of the excited photoelectron within a cluster (i.e., a group of atoms around an absorbing one) of a large size consisting of a few shells of atoms.[16] Within the dipole approximation, the x-ray-absorption coefficient $\alpha(E)$ for the K edge is proportional to both partial density of unoccupied Ni p symmetry states and squared dipole transition-matrix element, i.e.,

$$\alpha(E) \sim |m_L(E)|^2 N_p^{\mathrm{Ni}}(E), \tag{1}$$

here $N_p^{\mathrm{Ni}}(E)$ is the partial density of unoccupied Ni p-symmetry states, and

$$m_L(E) = \frac{\int dr\ \Phi_l(r,E)\Delta(r)\Psi_c(r)}{\left[\int dr\ \Phi_l(r,E)^2\right]^{1/2}} \tag{2}$$

is the normalized dipole transition matrix element, where $\Phi_l(r,E)$ is the solution of the radial Schrödinger equation at energy E for the muffin-tin potential ($l=1$ for the K edge), $\Delta(r)$ is the electron-photon interaction operator, $\Psi_K(r)$ is the Ni core K-level wave function. In our calculation, we have included phase shifts with orbital momentum up to 4 despite the fact that even for $l=3$ there is almost no change in the spectra in comparison with $l=2$.

RESULTS AND DISCUSSION

In Fig. 1 we present a comparison of the experimental x-ray-absorption spectra above the Ni K edge for Ni_3Al and $NiAl_3$ alloys. As one can see the spectra differ significantly. To perform theoretical analysis of these changes, we used the full multiple-scattering approach described above. The first step in the multiple-scattering analysis of XAFS data is to determine the size of a representative cluster of neighbor atoms around the absorbing Ni atom that will reproduce fully all of the fine structure of unoccupied electronic states in the conduction band of the alloy. As shown in Figs. 2 and 3, the analysis of the dependence of the main structures in XAFS spectra on cluster size shows that the convergence with cluster size is reached for a cluster with four shells (addition of the next shell has not resulted in variation of the spectra). This is not exactly true for Ni_3Al, where the addition of the fourth shell leads to further splitting of the fine-structure details. But these new fine details disappear when one takes

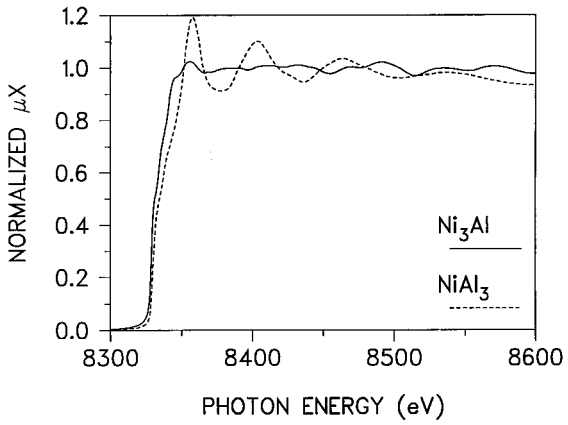

FIG. 1. Experimental x-ray-absorption spectra above the Ni K edge of Ni_3Al and $NiAl_3$.

into account all broadening factors that affect real experimental spectra and tend to smear the fine details in the spectra (will be discussed later in the text). Therefore, XAFS calculations to be compared with experimental data were performed by using this cluster size.

Another factor (beyond phase shifts and cluster local structure) that determines the XAFS in the multiple-scattering formalism is the transition-matrix element [Eq. (2)] that influences the relative intensity of XAFS features. In the previous section, we have shown that the K-edge x-ray absorption in the dipole approximation is proportional to the partial density of unoccupied Ni p states in the conduction band of the alloy. So, if the coefficient of proportionality (namely, the dipole matrix element [Eq. (2)]) is not a very sharp function of energy, as it is in the present case in the energy interval above 40 eV, one can to a first approximation study the details of the partial density of states, averaged in real space, by analyzing the fine structure of the x-ray-absorption spectra. In Figs. 4 and 5 we present the squared

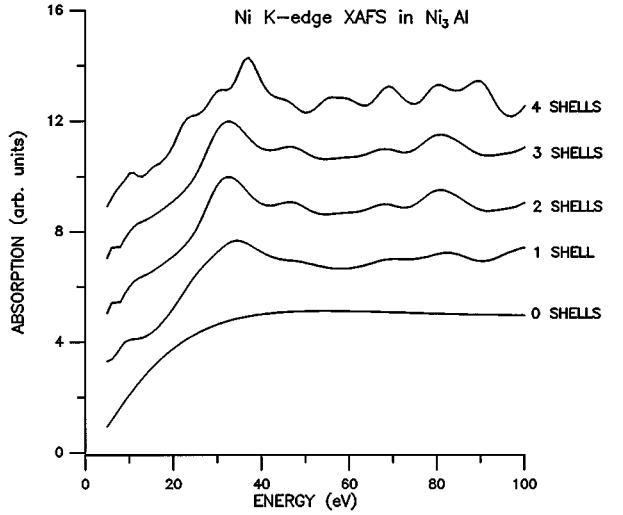

FIG. 2. X-ray-absorption coefficient for Ni K edge of Ni_3Al calculated within clusters of different size. Each spectrum is shifted along the y axis by a constant value in relation to the previous one. The zero of the energy scale is chosen at the average interstitial potential (i.e., muffin-tin zero) V_0 of the Ni atom. All spectra were obtained within the full multiple-scattering formalism.

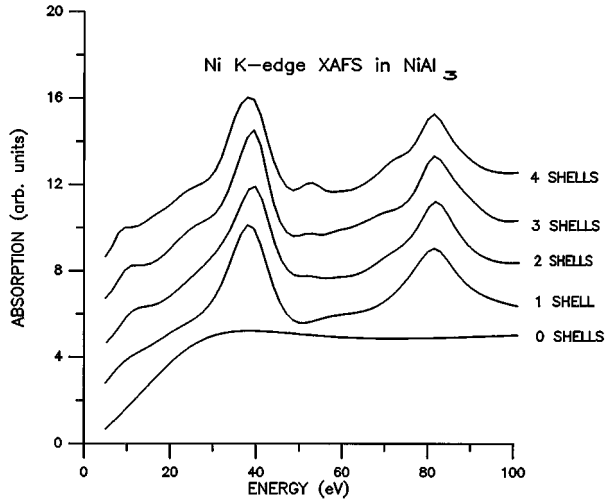

FIG. 3. X-ray-absorption coefficient for Ni K edge of $NiAl_3$ calculated within clusters of different size. Each spectrum is shifted along the y axis by a constant value in relation to the previous one. The zero of the energy scale is chosen at the average interstitial potential (i.e., muffin-tin zero) V_0 of the Ni atom. All spectra were obtained within the full multiple-scattering formalism.

dipole transition-matrix element $|m_L(E)|^2$ as a function of energy for both the ground-state potential (unrelaxed) and the potential including the core-hole effect (relaxed) corresponding to the x-ray-absorption process for both alloys. As one can see in the energy interval close to the absorption threshold the squared dipole transition-matrix element shows an energy dependence (strong enough in the energy interval from the main edge up to about 40 eV) and cannot be treated as a constant. However, the difference in the squared dipole transition-matrix element between the relaxed and the unrelaxed cases is not very significant in this case. In addition,

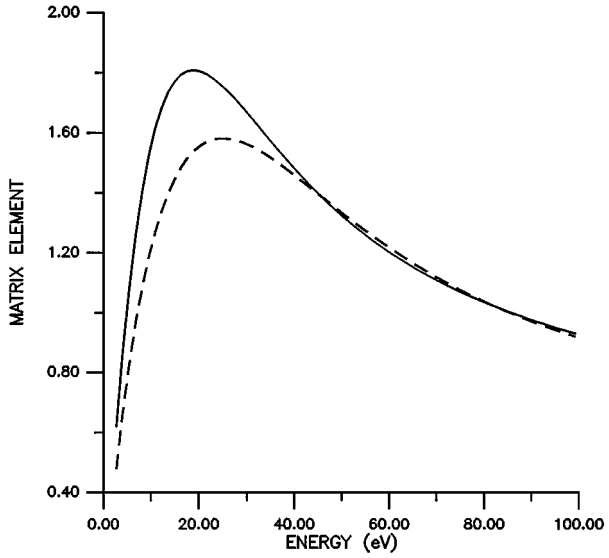

FIG. 4. Energy-dependent squared dipole transition-matrix elements, corresponding to the dipole Ni $1s \rightarrow \varepsilon p$ electronic transition in $NiAl_3$ for the ground-state potential of the central atom (unrelaxed) and taking into account the core-hole effect in the $Z+1$ approximation (relaxed) (unrelaxed, dashed line; relaxed, solid line).

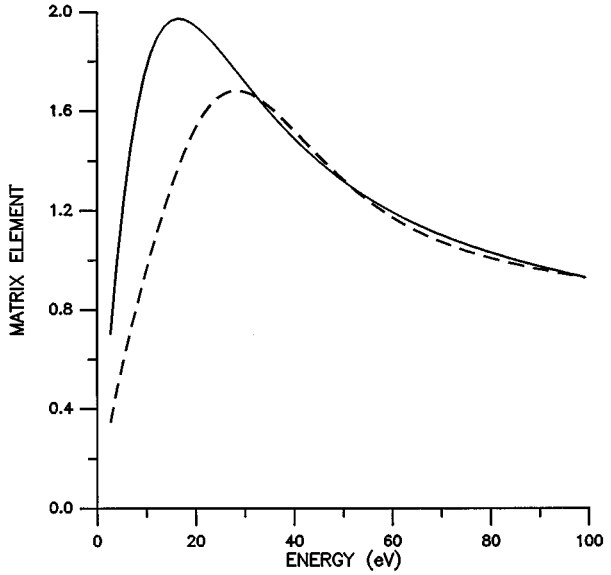

FIG. 5. Energy-dependent squared dipole transition-matrix elements, corresponding to the dipole Ni $1s \rightarrow \varepsilon p$ electronic transition in Ni_3Al for the ground-state potential of the central atom (unrelaxed) and taking into account the core-hole effect in the $Z+1$ approximation (relaxed) (unrelaxed, dashed line; relaxed, solid line).

there is not a large difference between the matrix elements of Ni_3Al and $NiAl_3$.

In order to perform the direct comparison with experimental data one must take into account two factors: the filling of occupied states following the Fermi distribution and the broadening of experimental spectra according to three factors: the core-hole lifetime, the finite mean-free path of the photoelectron, and the experimental resolution. We have used for the K core-hole bandwidth the value of 1.44 eV,[18] for the mean-free path of the photoelectron we have taken the energy-dependent function obtained in Ref. 19, and for the experimental energy resolution we used the value of 1.0 eV. We treated all of these factors as contributing to the imaginary part of the self-energy term that we use.

In Figs. 6 and 7 we present a comparison of experimental and theoretical Ni K-edge XAFS of Ni_3Al and $NiAl_3$, respectively. The theoretical spectra were calculated taking into account all of the broadening factors (see above) and the Fermi distribution. As one can see the agreement of theoretical results with experimental data is good enough for both alloys. Strictly speaking one must compare experimental data with theoretical calculation in relaxed potential (i.e., taking into account the presence of the core hole). This process was treated in the $Z+1$ approximation.[12] As one can see from Figs. 6 and 7, theoretical XAFS calculated in both the ground-state (unrelaxed) and the $Z+1$ (fully relaxed) approximation, for the case of the Ni K-edge absorption spectra, do not differ significantly (especially after taking into account all of the broadening factors) and both of the theoretical spectra are close to the experimental ones. Some small changes in relative intensity arise from the difference in the dipole transition-matrix elements calculated in the unrelaxed and the fully relaxed potentials (see Figs. 4 and 5). This situation is more or less general: for the K edges the contribution of the core hole is rather small,[20] while for the $L_{2,3}$ edges the core hole effect is significant.[21,22]

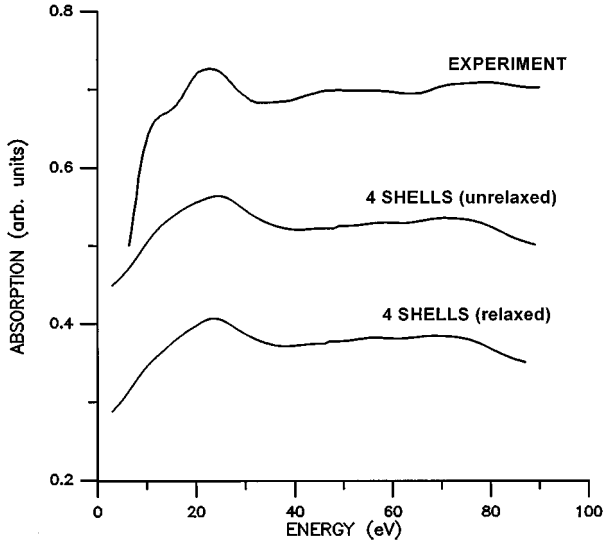

FIG. 6. Comparison of experimental and theoretical Ni K-edge XAFS of Ni_3Al. Theoretical spectrum is calculated taking into account all of the broadening factors and Fermi distribution (see text).

Our theoretical approach lets us calculate the curves of the partial Ni p density of states in the direction parallel to the c crystallographic vector and parallel to the ab plane. The results of such calculations are presented in Figs. 8 and 9. As one can see, these partial density of states curves are different along these two directions for both alloys.

CONCLUSIONS

We have applied a joint approach: experimental x-ray-absorption fine-structure measurements and their theoretical analysis on the basis of full multiple-scattering theory to study the peculiarities of the electronic structure of Ni_3Al and $NiAl_3$ alloys. The theoretical XAFS above the Ni K edge of Ni_3Al and $NiAl_3$ alloys calculated in the one-electron full

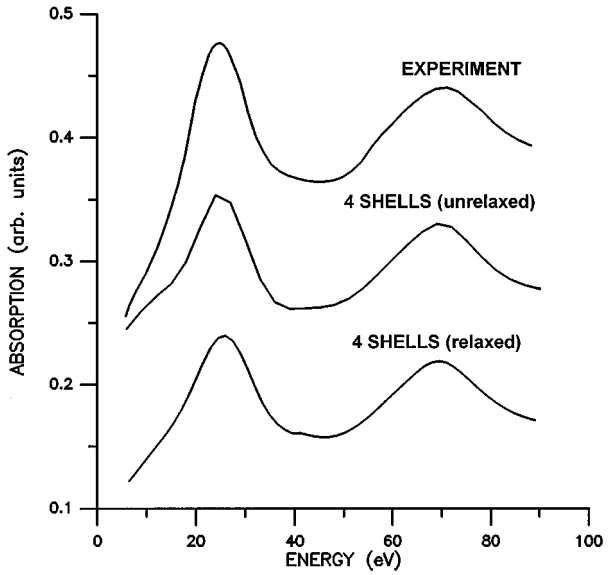

FIG. 7. Comparison of experimental and theoretical Ni K-edge XAFS of $NiAl_3$. Theoretical spectrum is calculated taking into account all of the broadening factors and Fermi distribution (see text).

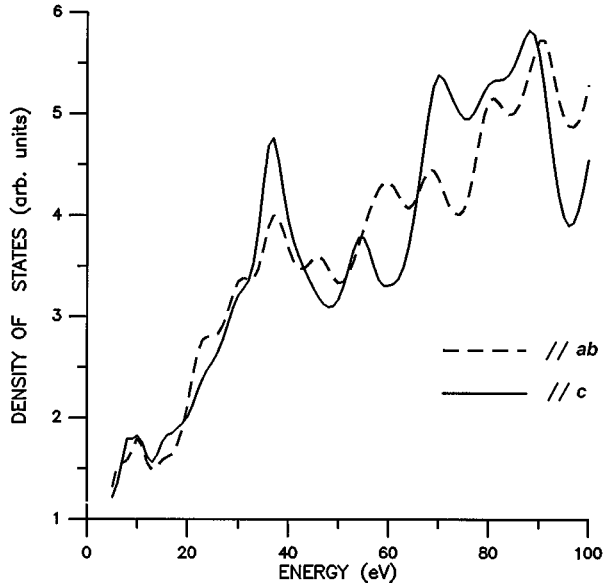

FIG. 8. The curves of Ni *p* unoccupied projected density of states in the direction parallel to the ***ab*** plane (dotted line) and parallel to the ***c*** axis (solid line) in Ni_3Al.

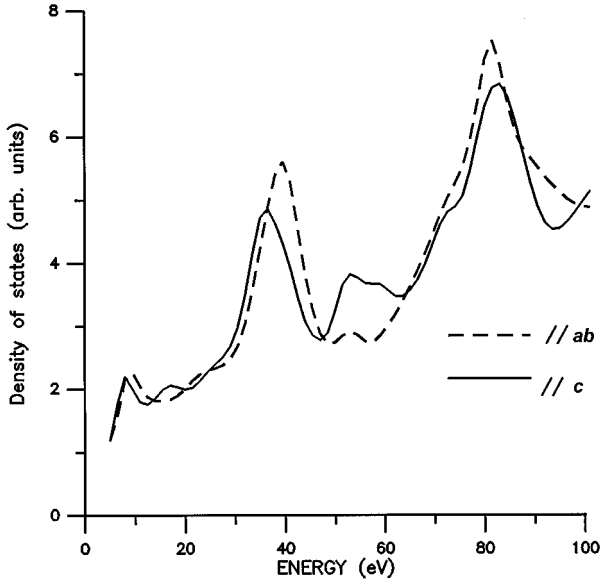

FIG. 9. The curves of Ni *p* unoccupied projected density of states in the direction parallel to the ***ab*** plane (dotted line) and parallel to the ***c*** axis (solid line) in $NiAl_3$.

multiple-scattering approach are found to be in agreement with experimental data. Due to the fact that the dipole transition-matrix element is not a very sharp function of energy in the interval above 40 eV, the experimental XAFS can be used to study the averaged in space partial Ni *p* unoccupied states in the conduction bands of the Ni_3Al and $NiAl_3$ alloys, showing their rather different electronic structure. Theoretical partial density of states curves calculated along the axis parallel to the **c** vector differ from the partial density of states curves calculated in the ***ab*** plane for both alloys. The difference in partial density of states in these two directions may cause different properties of the alloys along these directions and at least one can expect that if polarized spectra are measured, they may differ for these two directions.

ACKNOWLEDGMENTS

Research at NSWCCD was supported by the NSWCCD ILIR Program and at Rostov University it was partially supported by the Ministry of Science and Higher Education of Russia. The support of the U.S. Department of Energy, Division of Materials Sciences, under Contract No. DE-AS05-80-ER-10742 for its role in the development and operation of beam line X-11 at the National Synchrotron Light Source (NSLS) is acknowledged. The NSLS is supported by the U.S. Department of Energy, Division of Materials Sciences and Division of Chemical Sciences, under Contract No. DE-AC02-76CH00016.

*Author to whom all correspondence should be addressed.
†Electronic address: SOLDATOV@xafs.physfac.rnd.SU

[1] J. E. Payne and P. D. Desai, *Properties of Intermetallic Alloys I. Aluminides* (Center for Information and Numerical Data Analysis and Synthesis, Purdue University, West Lafayette, IN, 1994).
[2] J. J. Bergot, R. Caudron, P. Faivre, A. Lasalmonie, and P. Costa, J. Phys. (France) **35**, L225 (1974).
[3] D. Hackenbracht and J. Kubler, J. Phys. F **10**, 427 (1980).
[4] J. C. Fuggle, F. U. Hilleberecht, R. Zeller, Z. Zolnierek, and P. A. Bennett, Phys. Rev. B **27**, 2145 (1983).
[5] F. U. Hilleberecht, J. C. Fuggle, P. A. Bennett, and Z. Zolnierek, Phys. Rev. B **27**, 2179 (1983).
[6] P. A. Bennett, J. C. Fuggle, F. U. Hilleberecht, A. Lenselink, and G. A. Sawatzky, Phys. Rev. B **27**, 2194 (1983).
[7] J. R. Cuthill, A. J. McAliser, and M. L. Williams, J. Appl. Phys. **39**, 2204 (1968).
[8] G. Cubiotti, E. E. Krasovskii, O. V. Slobodyan, Yu. N. Kucherenko, and V. N. Antonov, J. Phys. Condens. Matter **7**, 4865 (1995).
[9] D. van der Marel and G. A. Sawatzky, Phys. Rev. B **37**, 10 674 (1988).
[10] Zs. Kovacs, L. Kover, P. Weightman, D. Varga, R. Sanjines, J. Palinkas, G. Margaritondo, and H. Adachi, Phys. Rev. B **54**, 8501 (1996).
[11] P. J. Durham, *X-ray Absorption: Principles, Applications and Techniques of EXAFS, SEXAFS and XAFS* (Wiley, New York, 1989), p. 53.
[12] A. Bianconi, *X-ray Absorption: Principles, Applications and Techniques of EXAFS, SEXAFS and XAFS* (Ref. 11), p. 537.
[13] D. E. Sayers, S. M. Heald, M. A. Pick, J. I. Budnick, E. A. Stern, and J. Wong, Nucl. Instrum. Methods Phys. Res. **208**, 631 (1983).
[14] K.-Q. Lu and E. A. Stern, Nucl. Instrum. Methods **212**, 475 (1983).
[15] E. A. Stern and K. Kim, Phys. Rev. B **23**, 3781 (1981).
[16] S. Della Longa, A. V. Soldatov, M. Pompa, and A. Bianconi, Comput. Mater. Sci. **4**, 199 (1995).
[17] R. W. G. Wyckoff, *Crystal Structure* (Interscience, New York, 1965); *Pearson's Handbook of Crystallographic Data for Intermetallic Phases*, edited by P. Villars and L. D. Calvert (American Society for Metals, Metals Park, OH, 1985), Vol. 2, p. 1038.

[18] *Unoccupied Electronic States*, edited by J. C. Fuggle and J. E. Inglesfield (Springer, Berlin, 1992).
[19] J. E. Muller, O. Jepsen, and J. W. Wilkins, Solid State Commun. **42**, 365 (1982).
[20] A. V. Soldatov, T. S. Ivanchenko, and A. Bianconi, J. Phys. Condens. Matter **5**, 7521 (1993).
[21] A. V. Soldatov, S. Della Longa, and A. Bianconi, Solid State Commun. **85**, 863 (1993).
[22] A. V. Soldatov, T. S. Ivanchenko, S. Della Longa, A. Kotani, Y. Iwamoto, and A. Bianconi, Phys. Rev. B **50**, 5074 (1994).